



Kinetic and Thermal Studies of Adsorption of Allura Red Dye by Surface Functionalized Magnetite Nanoparticles

JAIVEER SINGH^{1b}, ARTI JANGRA^{1b}, KEERTI RANI^{1b}, PARVIN KUMAR^{1b}, SURESH KUMAR^{1b} and RAMESH KUMAR^{*1b}

Department of Chemistry, Kurukshetra University, Kurukshetra-136119, India

*Corresponding author: E-mail: rameshkumarkuk@gmail.com

Received: 19 June 2021;

Accepted: 4 August 2021;

Published online: 20 October 2021;

AJC-20549

In the present study, chitosan functionalized magnetite nanoparticles (CS@MNPs) were synthesized by a simple and economical coprecipitation technique for efficient magnetic removal of allura red dye (ARD) by adsorption technique from the aqueous solution. Size and surface properties of the bare and surface functionalized MNPs were determined with the help of XRD and TEM technique. Surface functionalization of the bare MNPs was confirmed with the help of FT-IR spectroscopy and TGA techniques. Magnetic properties of the synthesized bare and functionalized MNPs were determined by VSM technique. The effect of various parameters including adsorbent dosages, contact time, temperature on adsorption capacity of the CS@MNPs for allura red dye were investigated with the help of UV-vis spectrophotometer. The pseudo second order kinetics and Langmuir adsorption isotherm model were found to fitted well with the adsorption process of dye onto the chitosan functionalized magnetite nanoparticles (CS@MNPs).

Keywords: Surface functionalized magnetite nanoparticles, Chitosan, Dye removal, Allura red dye.

INTRODUCTION

A huge amount of wastewater is produced in various industrial and domestic activities. Treatment and reprocessing of wastewater provide a way to control the wastage of water in the world. Hazardous dyes are among the major polluting content of wastewater [1]. Dyes are mostly used as a colouring agent in various industries such as food, textile, dyeing, paints, leather, paper and cosmetics industries [2-4]. The wastewater containing dye residuals from these industries is discharged into water streams. Studies all over the world reveals that around 10% of the total dye production is found in the wastewater. Dyes impart colour to water due to the presence of chromophores and has a serious hazard impact on the hydrosphere [5]. The functional groups present in the dyes help in their effective removal from the wastewater by using appropriate adsorbent. Allura red dye has sulfonate group as a main functional group. It is used in drugs, candies, jellies, sweets, cakes, juices, jams and cosmetics [6]. The harmful effects of this dye on human health have been reported by many studies [7]. So, it becomes necessary to remove this hazardous dye remnants from the wastewater in environmental favour. Adsorption technique is

a much easier and efficient technique for the removal of harmful pollutants including dyes from the wastewater [8]. For this purpose, various type of natural as well as synthetic adsorbents have been reported [9-11]. However, the adsorption of dye residuals from wastewater may be improved by using surface functionalized magnetic nanoparticles as the adsorbent.

In present paper, chitosan functionalized magnetite nanoparticles were used for the magnetic removal of allura red dye with the help of adsorption technique from aqueous solution. Furthermore, equilibrium and kinetic studies were carried out for adsorption process of allura red dye on the surface of chitosan loaded magnetite nanoparticles.

EXPERIMENTAL

All the chemicals used in present work were used without any purification and all were of analytical grade. Ammonia, hydrochloric acid, ferric chloride ($\text{FeCl}_3 \cdot 6\text{H}_2\text{O}$) and ferrous sulphate ($\text{FeSO}_4 \cdot 7\text{H}_2\text{O}$) were purchased from SRL Pvt. Ltd. (India). Chitosan was purchased from CDH Fine Chemical, India. Allura red dye was purchased from TCI. Deionized water was used through the experiments.

Synthesis and surface functionalization of magnetite nanoparticles: Conventional co-precipitation technique was used for the synthesis and surface functionalization of magnetite nanoparticles (MNPs) with chitosan as reported by Kumar *et al.* [12]. In brief, mixing of 5.8 g of ferric chloride and 3.2 g of ferrous sulphate salts were carried out in 100 mL of deionized water saturated with nitrogen gas with vigorous stirring (2000 rpm) followed by the addition of few drops of hydrochloric acid. The temperature of the reaction mixture was raised to ~ 90 °C. Nitrogen gas was bubbled throughout the reaction mixture in order to avoid oxidation of Fe^{2+} ions. After 0.5 h of vigorous stirring, 20 mL of ammonium hydroxide was added dropwise to the reaction mixture in order to carry out the coprecipitation of the iron salts. During the addition process of base to the reaction mixture the colour of the solution changed from light orange to black which confirmed the formation of magnetite nanoparticles. The surface functionalization of bare MNPs with chitosan was carried out by adding 50 mL of 0.5 g chitosan in 0.1 N acetic acid solution. Vigorous stirring with simultaneous nitrogen supply was further continued for ~ 1 h at 85-90 °C. The synthesized chitosan functionalized MNPs were decanted off from the aqueous solution with the help of strong magnet. The functionalized MNPs were washed 2-3 times with nitrogen saturated deionized water. The synthesized MNPs were dried in the vacuum oven at room temperature. The surface functionalization of bare magnetic nanoparticles can be represented pictorially as shown in Fig. 1.

Structural and magnetic characterization: Thermogravimetric analysis (TGA) in association with Fourier transform infrared spectroscopy (FTIR) was used for the structural characterization of the bare and surface functionalized MNPs. Transmission electron microscopy (TEM) technique was used for the average size determination and morphological studies of the synthesized MNPs. X-ray diffraction was used for the determination crystalline nature and verification of the average size of the obtained nanoparticles. Vibrating sample magnetometry (VSM) was used for the magnetic characterization of

both bare and surface modified MNPs. The XRD data of bare as well as functionalized MNPs were recorded between 20° to 80° angle range (2θ value) for the determination of their average size by using Debye-Scherrer equation [13]. The IR spectra of pure chitosan, bare and functionalized MNPs were recorded for the confirmation of successful coating on the surface of bare magnetite nanoparticles. Thermogravimetric studies were carried out between 30 to 500 °C (heating rate 10 °C/min). Vibrating sample magnetometer was used for recording the VSM data of the samples in a magnetic field up to 13,500 Oe at room temperature (298.15 K).

RESULTS AND DISCUSSION

FTIR studies: The presence of strong absorption band near 600 cm^{-1} in the spectra of bare and chitosan functionalized MNPs shows the presence of Fe-O bond, which is a characteristic peak for magnetite nanoparticles and this peak is absent in the IR spectrum of pure chitosan [14,15]. A broad peak in the higher wavenumber region *i.e.* from 3500 to 3200 cm^{-1} in the IR spectra of pure chitosan and chitosan functionalized Fe_3O_4 nanoparticles may be assigned to the O-H and N-H stretching vibration of the functional groups present in chitosan and this band is absent in the IR spectrum of bare MNPs [16]. Fig. 2a-c show IR spectra of unfunctionalized MNPs, pure chitosan and chitosan functionalized MNPs, respectively. In IR spectra of pure chitosan and chitosan functionalized MNPs, the IR bands in 2950 - 2850 cm^{-1} region may be assigned to C-H stretching vibrations present in the chitosan molecule while the bands in 1700 - 1500 cm^{-1} region corresponds to N-H bending vibrations. In addition to this, the bands in 1400 - 1100 cm^{-1} region may be due to C-N stretching vibrations and peaks between 1100 to 1000 cm^{-1} may be assigned to C-O-C stretching vibrations. These bands were absent in the spectrum of bare MNPs. A comparative study of these IR spectra shows a close resemblance in the bands observed in the IR spectrum of pure chitosan and that of chitosan functionalized MNPs.

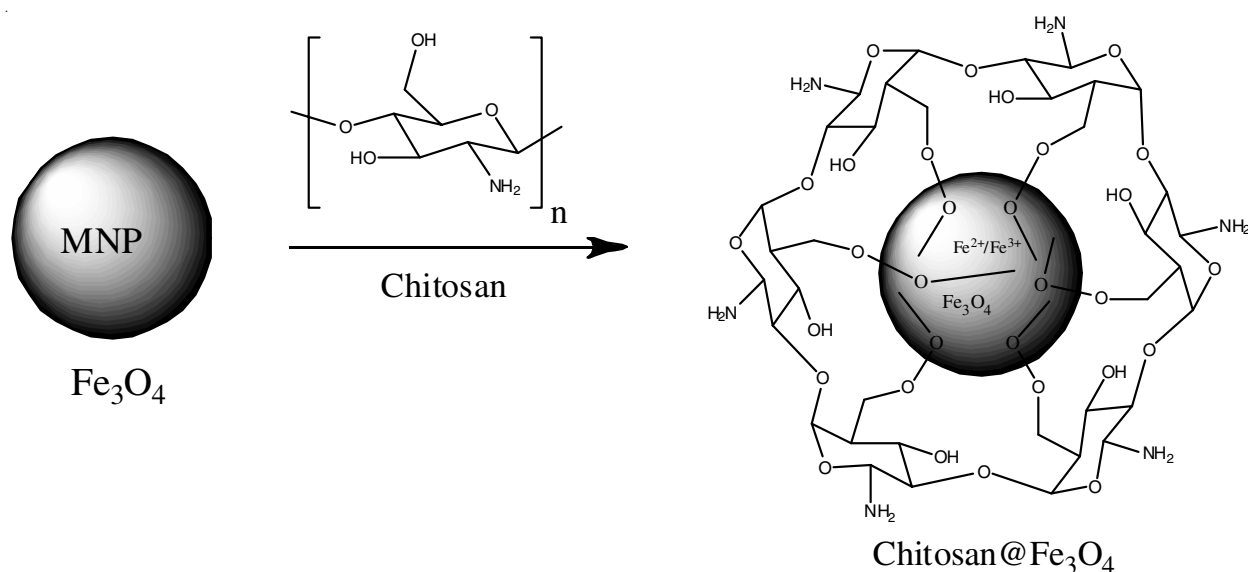


Fig. 1. Pictorial representation of surface functionalization of bare iron oxide nanoparticles with chitosan

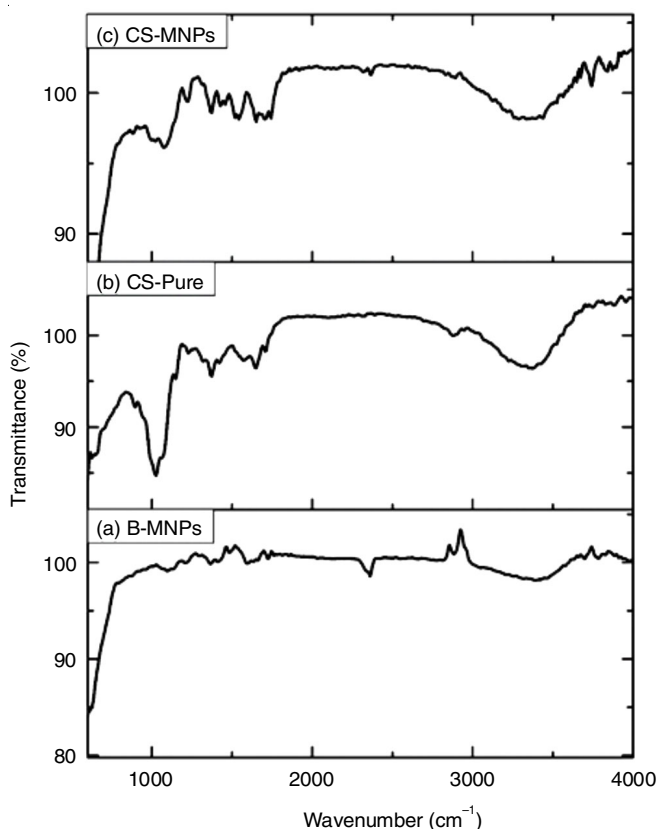


Fig. 2. FTIR spectrum of (a) bare MNPs (b) pure chitosan and (c) chitosan functionalized MNPs

This close resemblance of peaks confirmed the successful coating of chitosan on the surface of magnetite nanoparticles.

X-ray diffraction studies: The XRD diffraction pattern of Fe_3O_4 showed six major peaks at 30.4° , 35.54° , 43.23° , 53.37° , 57.37° and 63.42° . These peaks may be assumed to arise as a result of reflection from (2 2 0), (3 1 1), (4 0 0), (4 2 2), (5 1 1) and (4 4 0) crystal planes, respectively. The relative intensities of the peaks and their positions in the XRD diffractogram confirmed the cubic crystalline system of Fe_3O_4 nanoparticles. X-ray diffractogram of unfunctionalized (B-MNPs; Fig. 3a) and functionalized MNPs (CS-MNPs; Fig. 3b) exhibited the six common characteristic diffraction peaks of Fe_3O_4 , which helps to conclude safely that the basic crystal structure of magnetite nanoparticles remains unaffected by the surface functionalization of the core nanoparticles [17]. Further, the presence of these six basic characteristic peaks also confirms the inverse spinel structure with pure magnetite composition of the nanoparticles [18]. The mean size of nanoparticles was determined from the Scherrer equation [19] with the help of XRD peak broadening [20]. The reflection (3 1 1) was found to be the most intense peak of the XRD plot and hence the broadening of this peak was used for the calculation of the size of the nanoparticles. The average size of bare and chitosan functionalized MNPs was found to be 8.52 and 11.77 nm respectively, which are in close proximity with average size determined by the TEM studies.

Size and morphology of nanoparticles: The average diameter of bare (Fig. 4a) and chitosan functionalized MNPs

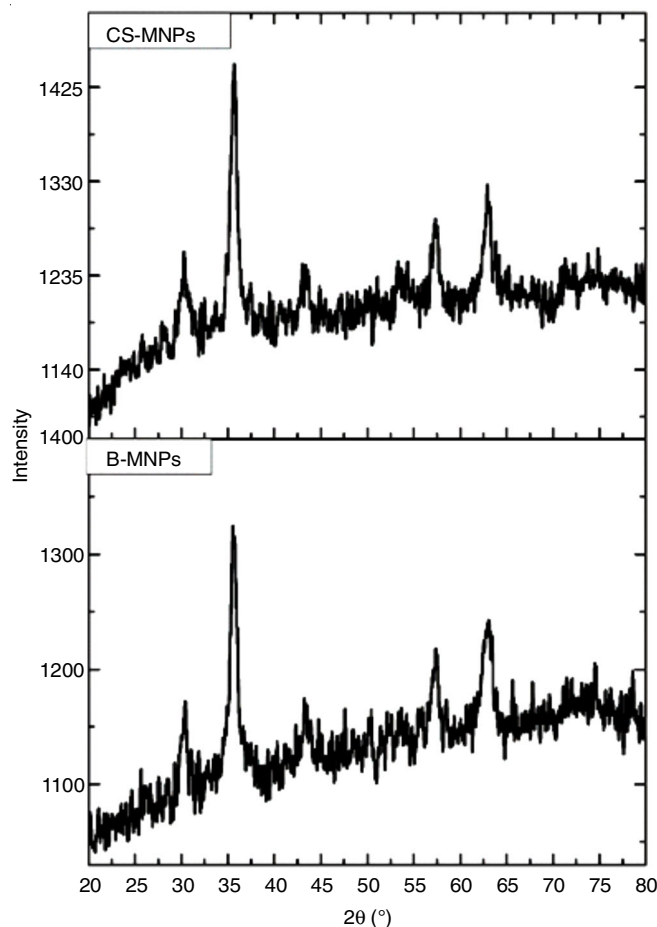


Fig. 3. XRD spectrum of bare MNPs (a) and chitosan functionalized MNPs (b)

(Fig. 4b) was found to be 10 nm and 14 nm, respectively as determined from the TEM studies. A close agreement of these results has been found with the results obtained with the Scherrer's equation from XRD plots. The increase in the average size of the surface functionalized nanoparticles after the functionalization process confirms the successful functionalization of bare MNPs with chitosan. The morphology of both bare and chitosan functionalized MNPs was observed to be nearly spherical.

Thermal analysis: The analytical technique of TG-DTA was used for the investigation of thermal behaviour of bare and chitosan functionalized MNPs. The comparison of the thermograms of bare, pure chitosan and chitosan functionalized MNPs confirmed the successful surface coating of bare MNPs. Fig. 5 shows the stacked thermogram of bare and chitosan functionalized MNPs. An initial weight loss of 6-7% was observed in the thermogram of bare MNPs up to 120°C , which may be due to the evaporation of water present in the sample. This initial weight loss pattern was found to be same for the chitosan functionalized MNPs, which may be similarly attributed to the desorption of water adsorbed by the sample [21]. The second stage of the weight loss was empty for the bare MNPs sample but a weight loss of around 14.8% was observed for the chitosan functionalized MNPs sample as the temperature was raised above 220°C . The decomposition and subsequent evaporation of coating layer may be assigned as the major

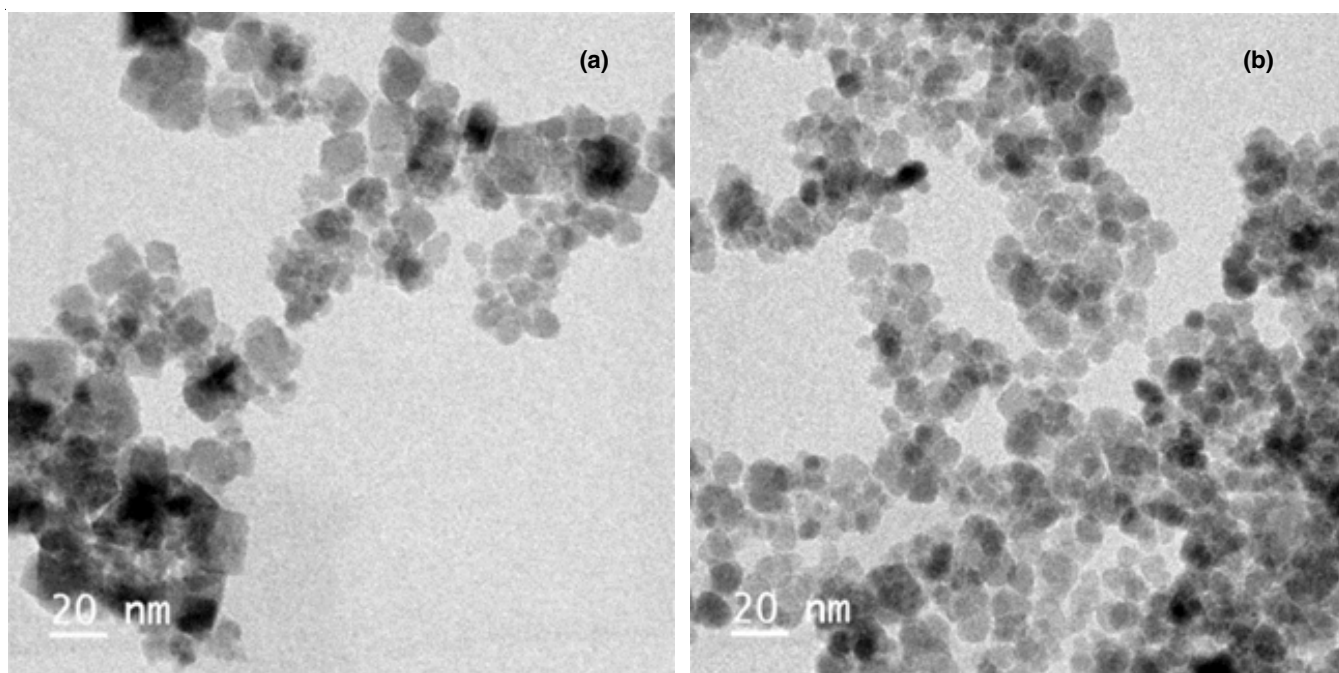


Fig. 4. TEM images of chitosan functionalized MNPs (a) and bare MNPs (b)

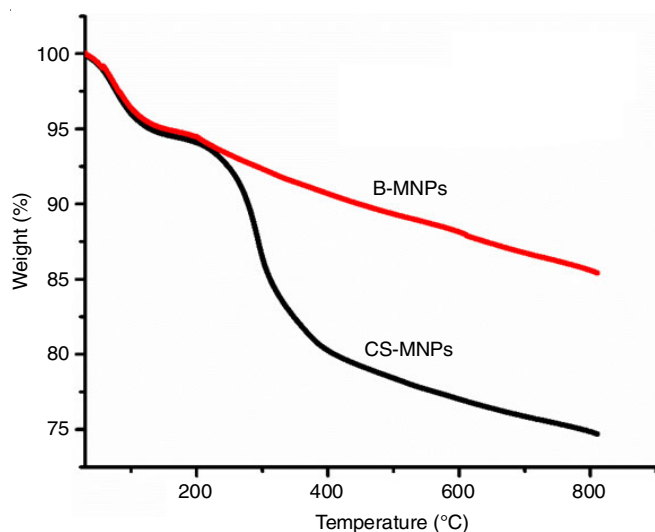


Fig. 5. Comparative analysis of thermogravimetric curves plots of bare and chitosan functionalized MNPs

reason for this abrupt weight loss for the chitosan functionalized MNPs sample. This comparison of TGA thermograms authorizes the successful covering of chitosan on the surface of bare MNPs. The TG curves of humic acid functionalized magnetite (11.4%) nanoparticles as well as methacrylic acid functionalized maghemite nanoparticles (12.0%) were also found to behave in a similar manner as reported earlier in the literature [22,23].

Magnetic properties of magnetite nanoparticles: The magnetic behaviour of the nanoparticles was found to be superparamagnetic in nature and it can be verified from the VSM studies of the samples. Further, the comparison of the VSM plots authenticate the fact that the magnetic behaviour of the nanoparticles remains unaffected after the surface functionalization of the bare nanoparticles. Fig. 6a-b show the VSM

plots {magnetization (M , emu/g) vs. magnetic field (H , Oe)} of bare and chitosan functionalized MNPs, respectively. The plots obtained for the samples of bare and chitosan functionalized MNPs have zero value coercivity or remanence *i.e.*, the net magnetization without external field was found to be zero for these samples, which authenticate the superparamagnetic nature of these synthesized nanoparticles [24]. The superparamagnetic nature of the samples may be assigned to the facts that the thermal fluctuations may become dominant over spontaneous magnetization at a given field [25]. In accordance to many studies carried on superparamagnetism it has been found that superparamagnetism is exhibited by nanoparticles due to their size effect (< 50 nm) and high crystallinity of the synthesized nanoparticles [13]. The magnetization saturation value of the samples was obtained by extrapolating the $1/H$ value to zero in the graph of M vs. $1/H$; where M is the magnetic saturation value and H is the value of applied magnetic field (inset plot in Fig. 6).

A magnetization saturation value of 1.66 emu/g was obtained for bare MNPs, which is in close proximity to the magnetization saturation value of bare MNPs as reported in the literature [15] and the magnetization saturation value for chitosan functionalized MNPs was obtained to be 1.35 emu/g. The slight difference in the value of magnetization saturation of the bare and chitosan functionalized MNPs samples may be justified due to the non-magnetic chitosan layer on the surface of MNPs. The lowering of the value of magnetization saturation of the chitosan functionalized MNPs may be assumed to be a result of exchange of electrons between the functional groups on chitosan and the surface iron atoms. In spite of all the differences, the point to be taken into consideration is that there is a slight difference in value of saturation magnetization of bare and chitosan functionalized MNPs, which suggests that chitosan functionalization did not affect the magnetic property

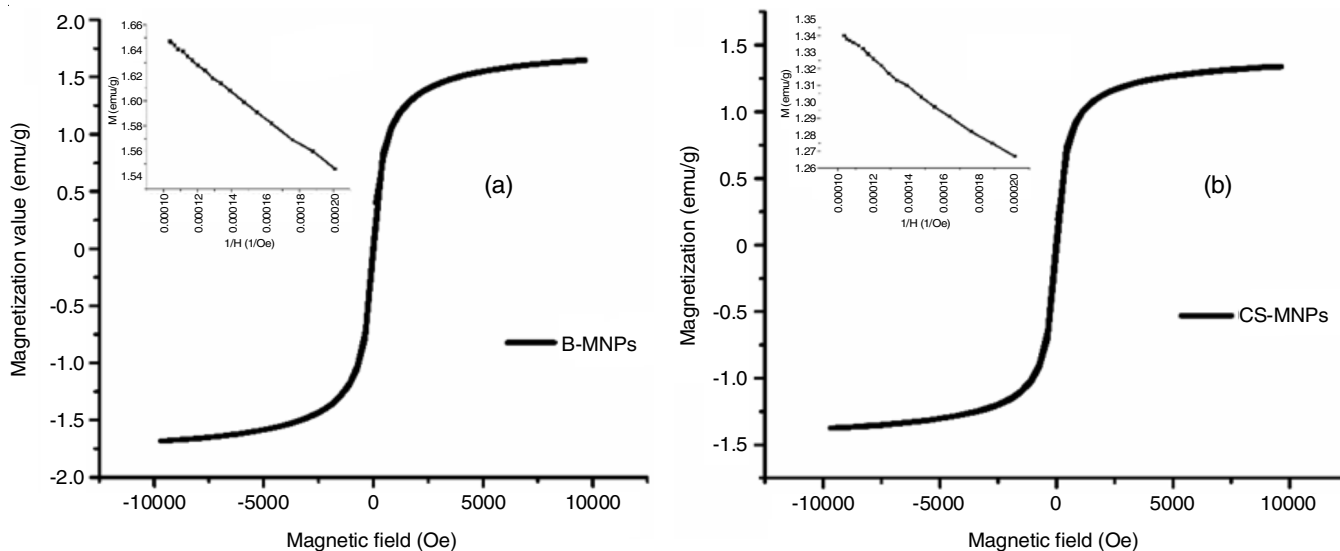


Fig. 6. VSM plots of (a) bare and (b) chitosan functionalized MNPs (plots of $1/H$ vs. M in the inset)

of bare MNPs significantly and their magnetic property may still be used. Further, a comparison of the obtained magnetization saturation values of bare (1.66 emu/g) and chitosan functionalized MNPs (1.35 emu/g) suggested that the content of chitosan in functionalized MNPs was about 18.674%, which was close to the value (14.8%) as determined by thermal analysis.

Adsorption dynamics

Effect of contact time: The process of adsorption has a direct relation with the contact time. The extent of adsorption increases with the increase in contact time. It becomes an important thing to know the equilibrium time for a certain adsorption process to perform various adsorption kinetic studies [26]. A calibration study was carried out for allura red dye to know the concentration of the unknown dye solution in the range of 10 to 60 mg/L. In order to determine the equilibrium time for the adsorption of allura red dye from the aqueous solution by chitosan functionalized MNPs, a fix amount of chitosan functionalized MNPs (100 mg) was put into 250 mL of allura red dye solution (60 mg/L). The pH and temperature of the solution was maintained constant (6.8; 298 K). The mixture was put on stirring at a rate of 400 rpm after 5 min ultrasonication. A fix amount of the mixture at some predetermined time intervals were taken out for the determination of amount of dye adsorbed by chitosan functionalized MNPs at that instant of time. Chitosan functionalized MNPs were separated with the help of a permanent magnet from the solution and the absorbance of the decanted solution was determined by a UV/visible spectrophotometer at maximum absorbance wavelength of allura red dye (500 nm). Knowing the absorbance of the decanted dye solution, the residual amount of the dye can be easily determined with the help of calibration curve (Fig. 7) of allura red dye.

The amount of the dye adsorbed per gram of nanoparticles (q_t) can be determined with the help of eqn. 1 [26]:

$$q_t = \frac{C_i - C_f}{W} \times V \quad (1)$$

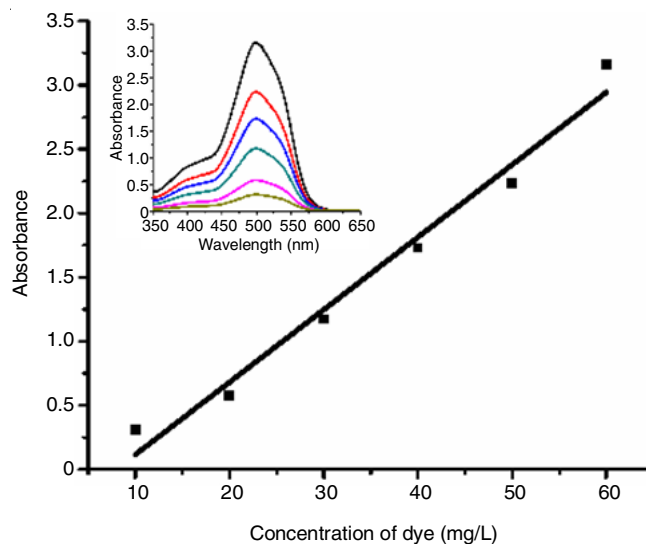


Fig. 7. Calibration curve for allura red dye (10 to 60 mg/L)

where the initial and final concentrations of allura red dye (mg/L) are denoted by C_i and C_f , respectively, W denotes the weight (g) of chitosan functionalized nanoparticles, q_t represents the adsorbed amount of dye per gram of the adsorbent (mg/g) and the volume of the solution (L) is denoted by V .

The time taken for the adsorption to reach the equilibrium point depends on the nature of adsorbed molecules and the adsorbent. Fig. 8 represents the effect of contact time on the adsorption of allura red dye by chitosan functionalized MNPs. The initial dye concentration for the whole process was 60 mg/L (C_0), the temperature was maintained to 25 °C and the pH of the solution was 6.80. From the graph, it has been found that the adsorption of allura red dye increased sharply in the first 90 min after that the adsorption equilibrated at about 115 min. Therefore, all adsorption kinetic studies for the samples under study were carried out by considering an optimum time period of 170 min as equilibrium time.

Effect of adsorbent dosages: The effectiveness of adsorbent for the removal of dye is an important aspect in dye removal

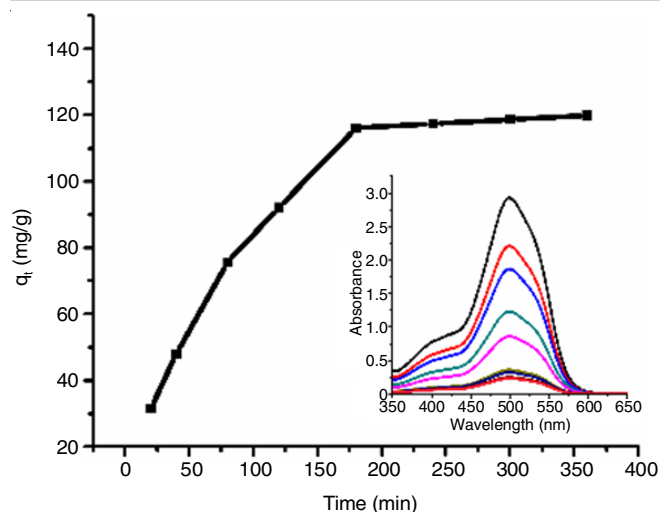


Fig. 8. Plot of amount of dye adsorbed (mg/g) per gram of adsorbent versus time

processes. An optimum amount of adsorbent required for the efficient removal of dye can be easily determined by studying the effect of varying adsorbent dosages for the removal of a fix concentration of dye from the aqueous solution. Fig. 9 shows the plot of amount of dye adsorbed per gram of the adsorbent (mg/g) versus the amount of adsorbent used (mg/L).

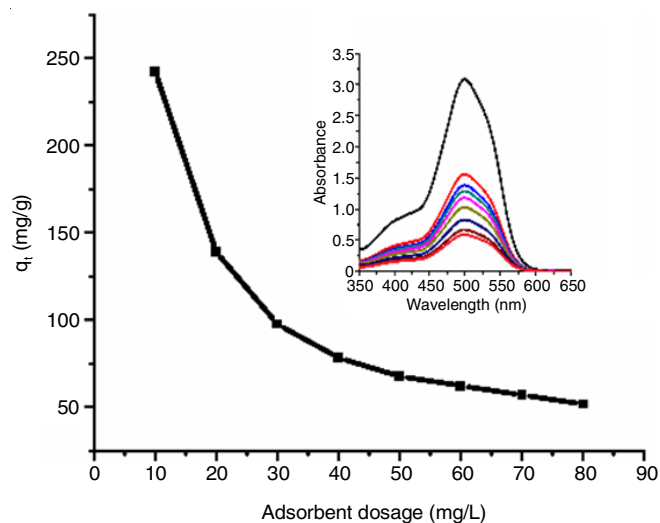


Fig. 9. Plot of amount of dye adsorbed (mg/g) vs. amount of adsorbent used (mg/L)

Removal efficiency: Further, the removal efficiency (%) was calculated by the expression in eqn. 2 [27]:

$$R (\%) = \frac{C_i - C_e}{C_i} \times 100 \quad (2)$$

where, R is the removal efficiency, C_0 and C_e (mg/L) are the concentrations of allura red dye at the initial and equilibrium states, respectively. The plot of removal efficiency against the amount of adsorbent used has also been plotted (Fig. 10).

Kinetics model fitting: The mechanism of kinetics of the adsorption process can be made easily understandable with the help of the kinetic models [27]. The kinetic data of the

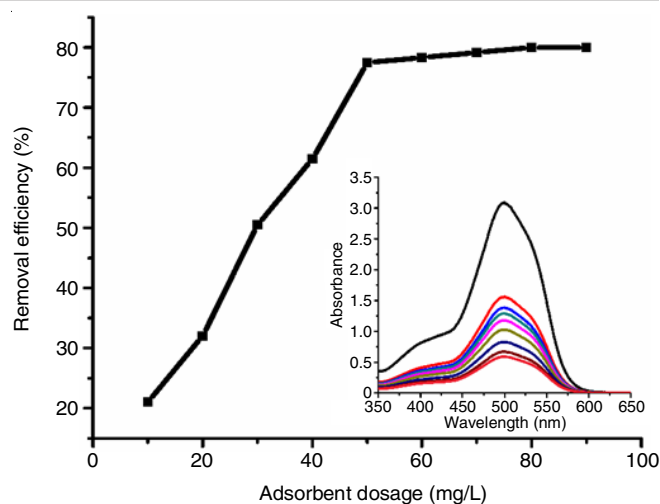


Fig. 10. Plot of removal efficiency of dye (%) versus amount of adsorbent used (mg/L)

adsorption was fitted to the kinetic adsorption models. The kinetics model which fitted best to the adsorption process used to understand the mechanism of the adsorption process. The experimental data of the adsorption of allura red dye on to the chitosan functionalized MNPs were fitted to the pseudo-first order and pseudo-second order kinetic models.

Pseudo first order kinetics: Eqn. 3 represents the kinetic equation for the pseudo first order kinetic model [28]:

$$\ln(q_e - q_t) = \ln q_e - k_1 t \quad (3)$$

In this equation, the amount of allura red dye adsorbed per gram of chitosan functionalized MNPs at any instant of time is represented by q_t (mg/g), the amount of allura red dye adsorbed per gram of chitosan functionalized MNPs at equilibrium is represented by q_e (mg/g) and the equilibrium rate constant for the pseudo first order kinetic model is represented by k_1 (min^{-1}). Fig. 11 shows the least square fitted plot of $\ln(q_e - q_t)$ versus time.

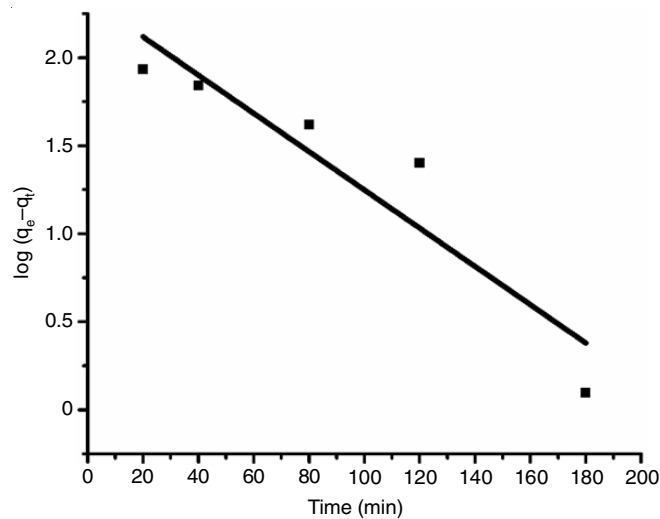


Fig. 11. Plot of $\log(q_e - q_t)$ against time

Pseudo second order kinetics: Eqn. 4 represents the kinetic equation for pseudo-second order process [29].

$$\frac{t}{q_t} = \frac{1}{k_2 q_e^2} + \frac{t}{q_e} \quad (4)$$

In this equation, the amount of allura red dye absorbed any instant of time t is represented by q_t (mg/g), the amount of dye adsorbed on the surface of adsorbent per gram of the adsorbent at equilibrium is represented by q_e (mg/g) and the equilibrium rate constant for pseudo-second-order model is represented by k_2 ($g\ mg^{-1}\ min^{-1}$). Fig. 12 represents the least square fitted plot of t/q_t versus time.

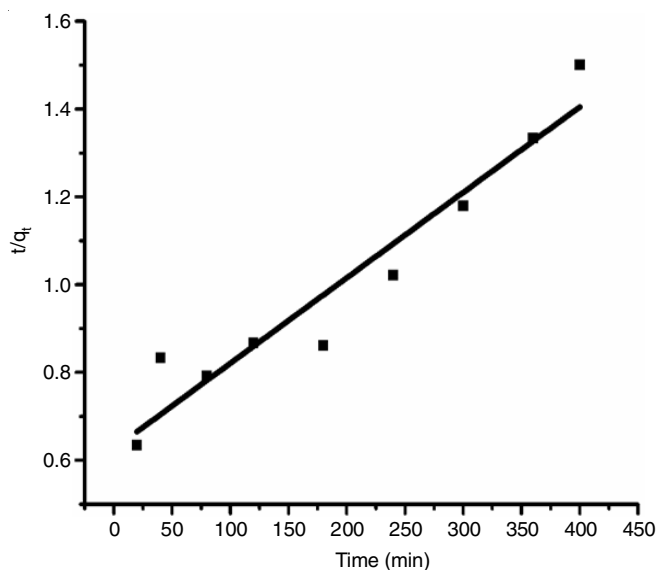


Fig. 12. Plot of t/q_t against time

The least square fitted curve for both pseudo-first-order and pseudo-second-order were compared and it has been found from the correlation coefficients of both the curve which are 0.83308 and 0.91646, respectively, that the pseudo-second-order model fitted better fit than the pseudo-first order model. Table-1 represents the kinetic parameters and rate constants for both the models.

Equilibrium adsorption isotherm experiment of chitosan functionalized MNPs with allura red dye

Effect of temperature: The adsorption isotherm model has an important role for designing the adsorption system for a particular adsorption process for the efficient removal of the dye. So, it becomes important to assign a particular adsorption isotherm model to a particular adsorption process. The adsorption isotherm model also helps to understand the adsorption mechanism of the adsorption process, which in turn helps to design the best strategy for the removal of dye solution. The adsorption isotherm model which fitted best to the adsorption process can be determined by the study of temperature dependency of adsorption process. Langmuir adsorption is a monolayer adsorption while Freundlich adsorption is a multilayer adsorption model. Langmuir model treats all the sites on the adsorbent surface equivalent both geometrically as well as energetically. The adsorption isotherms of allura red dye onto chitosan functionalized MNPs at different temperatures are given in Fig. 13.

According to Langmuir model neighbouring site does not have any effect on the adsorption process at a particular site. Freundlich model consider all the adsorption sites heterogen-

Pseudo-first-order model			Pseudo-second-order model		
R^2	k_1 (min^{-1})	q_e (mg/g)	R^2	k_2 ($g\ mg^{-1}\ min^{-1}$)	q_e (mg/g)
0.83308	1.01087×10^{-2}	10.3287	0.91646	6.0701×10^{-6}	512.82

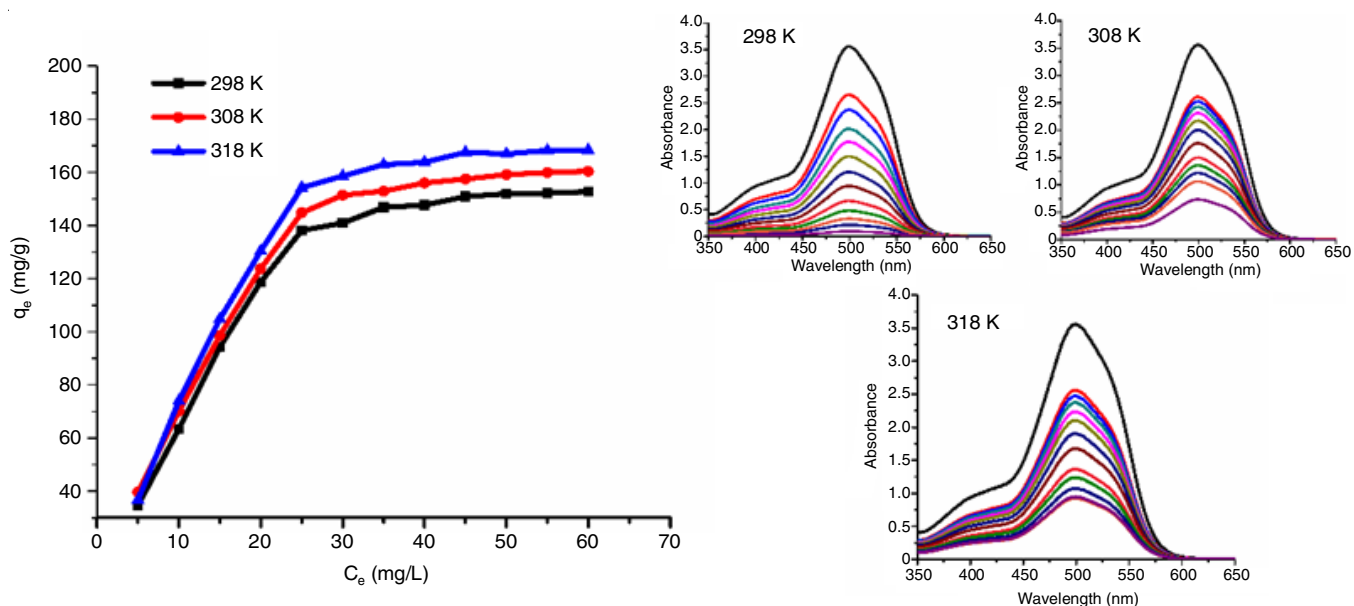


Fig. 13. Plot of amount of dye adsorbed per gram of the adsorbent with amount of adsorbent used at three different temperature

eous and the adsorption energy decreases exponentially with the adsorption layers. Adsorption data for the removal of allura red dye was recorded at various temperatures for obtaining the adsorption isotherms.

Langmuir isotherm: Langmuir isotherm model is based on the monolayer adsorption of dye molecule on the fixed distinct sites of the adsorbent. In Langmuir isotherm there is no neighbouring transmigration of the adsorbate in the plane of surfaces and the energies of adsorption has been found as uniform throughout. The equation used to express Langmuir adsorption isotherm has been stated in eqn. 5 [28]:

$$\frac{C_e}{q_e} = \frac{1}{k_L q_m} + \frac{C_e}{q_m} \quad (5)$$

In this equation, the equilibrium concentration of allura red dye solution (mg/L) is represented by C_e , the amount of allura red dye adsorbed per gram of the chitosan functionalized MNPs at the equilibrium is represented by q_e (mg/g), the maximum adsorption amount is represented by q_o (mg/g) and the Langmuir binding constant is represented by k_L , which is related to the energy of adsorption. Fig. 14 shows the straight-line plot of C_e/q_e versus C_e .

The correlation coefficient as determined from the last square fitted curve of the Langmuir adsorption isotherm (C_e/q_e against C_e) at 298 °C is $R^2 = 0.95223$. The value of q_m obtained from the Langmuir isotherm is 213.220 mg/g at 298 °C, which is in good consistency with the experimental data and supports the adsorption process to be mainly a monolayer adsorption process.

Freundlich isotherm: The Freundlich adsorption isotherm model considers the process of adsorption as multilayer, the sites of the adsorption on the adsorbents are heterogeneous in nature and the energy of the adsorption has an exponential decay with the adsorption layers. The equation used to express the Freundlich adsorption isotherm model can be stated as in eqn. 6 [29]:

$$\ln q_e = \ln k_f + b_f \ln C_e \quad (6)$$

In this equation, the amount of allura red dye adsorbed per gram of the chitosan functionalized MNPs at the equilibrium is represented by q_e (mg/g), the Freundlich constant is represented by k_f , the adsorption intensity is represented by constant b_f , the equilibrium concentration of allura red dye solution is represented by C_e (mg/L). Fig. 15 represents the least square fitted plots of $\ln q_e$ versus $\ln C_e$. The correlation coefficient obtained from the least square fitted curves of Freundlich adsorption isotherm at 298 °C is $R_2 = 0.88388$, which in comparison to the Langmuir adsorption isotherm does not fit the Freundlich model very well. The adsorption isotherm parameters are presented in Table-2.

Thermodynamics of adsorption of ARD on chitosan functionalized MNPs: From the thermodynamic parameters, determined from the equilibrium studies, it has been found that ΔG° value is negative and hence the adsorption process is spontaneous in nature (Table-3). Fig. 16 shows the linear plot of $\ln K_c$ versus $1/T$ [30] as according to eqn. 7:

$$\ln K_c = \frac{\Delta S^\circ}{R} - \frac{\Delta H^\circ}{RT} \quad (7)$$

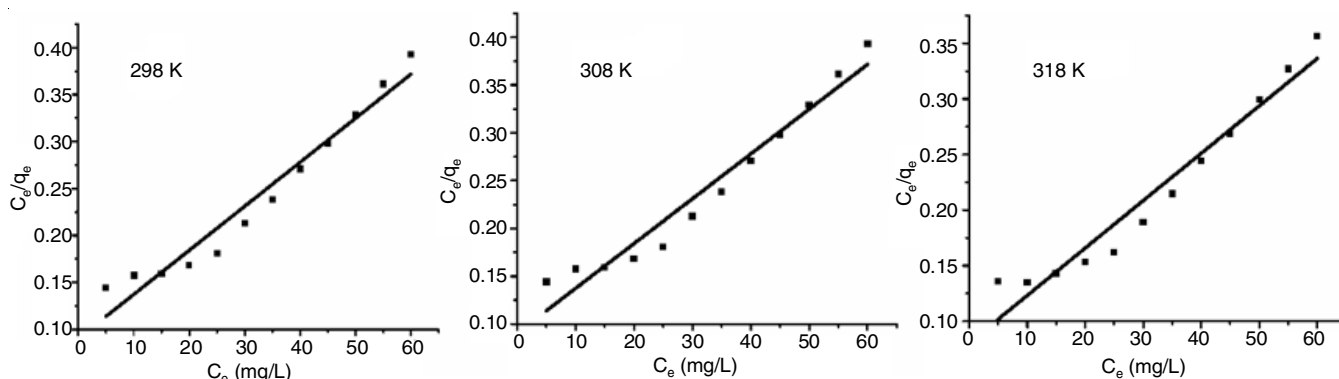


Fig. 14. Plot of C_e/q_e against C_e at three different temperatures

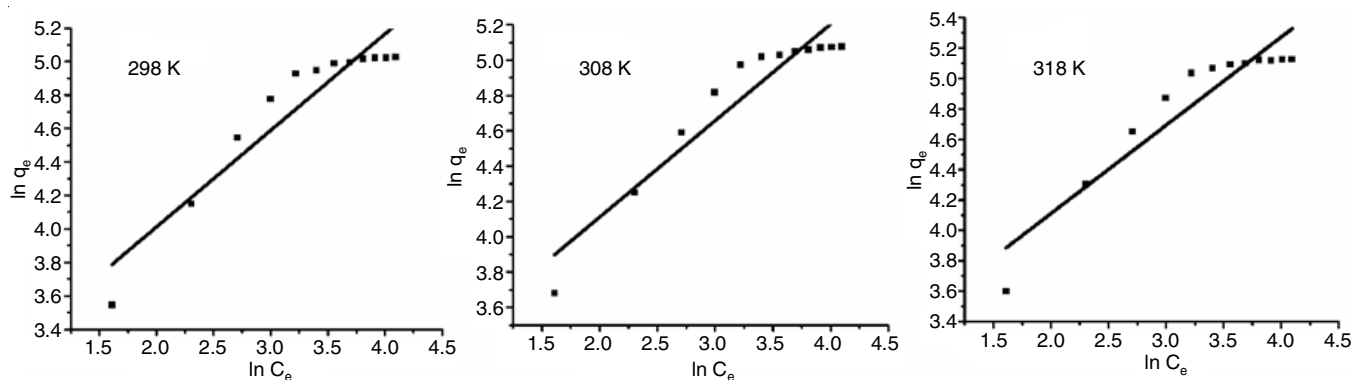


Fig. 15. Plot of $\ln q_e$ against $\ln C_e$ at three different temperatures

TABLE-2
LANGMUIR AND FREUNDLICH PARAMETERS FOR THE ADSORPTION OF
ALLURA RED DYE ON CHITOSAN FUNCTIONALIZED MNPs

Temp. (K)	Langmuir model			Freundlich model		
	R ²	q _m (mg/g)	k _L (L/mg)	R ²	k _f	b _f
298	0.95223	213.2196	0.0518968	0.88388	17.460	0.5765
308	0.96513	217.3913	0.0573855	0.89134	20.455	0.5466
318	0.94616	234.7418	0.0527965	0.87156	19.150	0.5799

TABLE-3
THERMODYNAMICS ADSORPTION PARAMETERS FOR
THE ADSORPTION OF ALLURA RED DYE ON CS-MNPs

Temp. (K)	ΔG° (kJ/mol)	ΔH° (kJ/mol)	ΔS° (J/(mol K))
298	-0.671		
308	-0.658	-1.0496	-1.2720
318	-0.404		

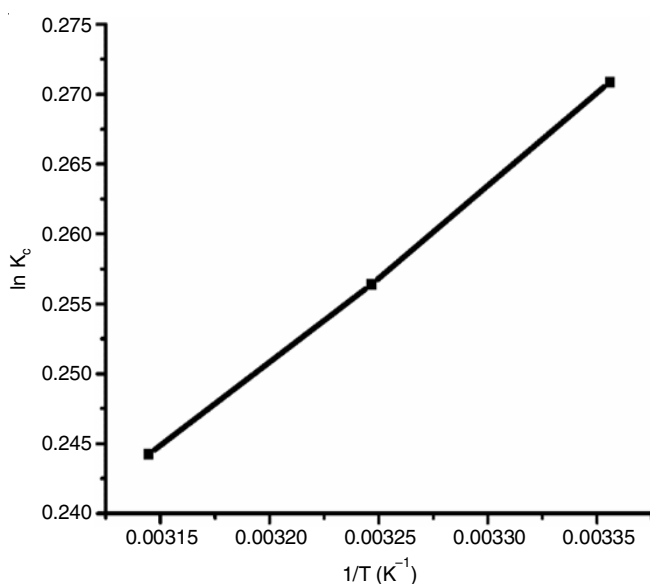


Fig. 16. Linear plot of van't Hoff equation

Conclusion

Chitosan functionalized magnetite nanoparticles were successfully synthesized and used for the adsorption of allura red dye from the aqueous solution. The kinetics of adsorption has been studied and found to be more compatible with the pseudo-second-order mechanism. Further, the equilibrium studies have been carried out for adsorption isotherm model fitting. Langmuir isotherm model was comparatively found to be better fitted with the experimental results.

ACKNOWLEDGEMENTS

One of the authors, Jaiveer Singh is thankful to UGC, New Delhi for granting the financial aid in the form of UGC-SRF fellowship.

CONFLICT OF INTEREST

The authors declare that there is no conflict of interests regarding the publication of this article.

REFERENCES

- L.D. Ardila-Leal, R.A. Poutou-Piñales, A.M. Pedroza-Rodríguez and B.E. Quevedo-Hidalgo, *Molecules*, **26**, 3813 (2021); <https://doi.org/10.3390/molecules26133813>
- H.B. Slama, A.C. Bouket, Z. Pourhassan, F.N. Alenezi, A. Silini, H. Cherif-Silini, T. Oszako, L. Luptakova, P. Golinska and L. Belbahri, *Appl. Sci.*, **11**, 6255 (2021); <https://doi.org/10.3390/app11146255>
- K.G. Pavithra, P.S. Kumar, V. Jaikumar and P.S. Rajan, *J. Ind. Eng. Chem.*, **75**, 1 (2019); <https://doi.org/10.1016/j.jiec.2019.02.011>
- M. Yusuf, M. Shabbir and F. Mohammad, *Nat. Prod. Bioprospect.*, **7**, 123 (2017); <https://doi.org/10.1007/s13659-017-0119-9>
- S. Gita, A. Hussan and T.G. Choudhury, *Environ. Ecol.*, **35**, 2349 (2017).
- K. Rovina, S. Siddiquee and S.M. Shaarani, *Front. Microbiol.*, **7**, 798 (2017); <https://doi.org/10.3389/fmicb.2016.00798>
- T. Tanaka, *Toxicology*, **92**, 169 (1994); [https://doi.org/10.1016/0300-483X\(94\)90175-9](https://doi.org/10.1016/0300-483X(94)90175-9)
- V. Katheresan, J. Kansedo and S.Y. Lau, *J. Environ. Chem. Eng.*, **6**, 4676 (2018); <https://doi.org/10.1016/j.jece.2018.06.060>
- R.V. Kandisa, N. Saibaba KV, K.B. Shaik and R. Gopinath, *J. Bioremed. Biodegrad.*, **7**, 371 (2016); <http://doi.org/10.4172/2155-6199.1000371>
- N.B. Singh, G. Nagpal, S. Agrawal and Rachna, *Environ. Technol. Innov.*, **11**, 187 (2018); <https://doi.org/10.1016/j.eti.2018.05.006>
- M. Batool, M.Z. Qureshi, F. Hashmi, N. Mehboob and W.M. Daoush, *Asian J. Chem.*, **31**, 707 (2019); <https://doi.org/10.14233/ajchem.2019.21752>
- R. Kumar, B.S. Inbaraj and B.H. Chen, *Mater. Res. Bull.*, **45**, 1603 (2010); <https://doi.org/10.1016/j.materresbull.2010.07.017>
- X.N. Pham, T.P. Nguyen, T.N. Pham, T. Thuy, N. Tran and T.V.T. Tran, *Adv. Nat. Sci.: Nanosci. Nanotechnol.*, **7**, 045010 (2016); <http://doi.org/10.1088/2043-6262/7/4/045010>
- L. Cabrera, S. Gutierrez, N. Menendez, M.P. Morales and P. Herrasti, *Electrochim. Acta*, **53**, 3436 (2008); <https://doi.org/10.1016/j.electacta.2007.12.006>
- D. Maity and D.C.Á. Agrawal, *J. Magn. Magn. Mater.*, **308**, 46 (2007); <https://doi.org/10.1016/j.jmmm.2006.05.001>
- T. Saba, F. Minhas, M.I. Malik, F.N. Talpur, A. Jabbar and M.I. Bhangar, *Am. J. Anal. Chem.*, **9**, 633 (2018); <https://doi.org/10.4236/ajac.2018.912046>
- W. Wu, Z. Wu, T. Yu, C. Jiang and W.S. Kim, *Sci. Technol. Adv. Mater.*, **16**, 023501 (2015); <https://doi.org/10.1088/1468-6996/16/2/023501>
- C. Pan, B. Hu, W. Li, Y. Sun, H. Ye and X. Zeng, *J. Mol. Catal., B Enzym.*, **61**, 208 (2009); <https://doi.org/10.1016/j.molcatb.2009.07.003>
- G. Unsoy, R. Khodadust, S. Yalcin, P. Mutlu and U. Gunduz, *Eur. J. Pharm. Sci.*, **62**, 243 (2014); <https://doi.org/10.1016/j.ejps.2014.05.021>
- G. Li, Y. Jiang, K. Huang, P. Ding and J. Chen, *J. Alloys Compd.*, **466**, 451 (2008); <https://doi.org/10.1016/j.jallcom.2007.11.100>

21. N.A. Kalkan, S. Aksoy, E.A. Aksoy and N. Hasirci, *J. Appl. Polym. Sci.*, **124**, 576 (2012); <https://doi.org/10.1002/app.34986>
22. R.K. Gautam and I. Tiwari, *Chemosphere*, **245**, 125553 (2020); <https://doi.org/10.1016/j.chemosphere.2019.125553>
23. Z. Shan, W.-S. Yang, X. Zhang, Q.-M. Huang and H. Ye, *J. Braz. Chem. Soc.*, **18**, 1329 (2007); <https://doi.org/10.1590/S0103-50532007000700006>
24. M. Yamaura, R.L. Camilo, L.C. Sampaio, M.A. Macêdo, M. Nakamura and H.E. Toma, *J. Magn. Magn. Mater.*, **279**, 210 (2004); <https://doi.org/10.1016/j.jmmm.2004.01.094>
25. S. Sun, H. Zeng, D.B. Robinson, S. Raoux, P.M. Rice, S.X. Wang and G. Li, *J. Am. Chem. Soc.*, **126**, 273 (2004); <https://doi.org/10.1021/ja0380852>
26. O. Keskinan and B. Balci, *Asian J. Chem.*, **25**, 4693 (2013); <https://doi.org/10.14233/ajchem.2013.14942>
27. S. Jemimah and S.R. Bheeter, *Asian J. Chem.*, **29**, 535 (2017); <https://doi.org/10.14233/ajchem.2017.20225>
28. A.A. Al-Arfaj, F. Alakhras, E. Al-Abbad, N.O. Alzamel, N.A. Al-Omair and N. Ouerfelli, *Asian J. Chem.*, **30**, 1645 (2018); <https://doi.org/10.14233/ajchem.2018.21298>
29. M.A. Shaker, A.A. Yakout, D.A. El-Hady, A.H. Abdel-Salam and H.M. Albishri, *Asian J. Chem.*, **27**, 4397 (2015); <https://doi.org/10.14233/ajchem.2015.19142>
30. L. Zhou, J. Jin, Z. Liu, X. Liang and C. Shang, *J. Hazard. Mater.*, **185**, 1045 (2011); <https://doi.org/10.1016/j.jhazmat.2010.10.012>